Physica E 144 (2022) 115413

Contents lists available at ScienceDirect

Physica E: Low-dimensional Systems and Nanostructures

journal homepage: www.elsevier.com/locate/physe

Spin-dependent transport and spin transfer torque in a system based on silagraghene nanoribbons

M.Kh. Maher [a], M.R. Roknabadi [a,*], M. Behdani [a], N. Shahtahmassebi [a,b]

[a] Department of Physics, Ferdowsi University of Mashhad, Iran
[b] Nanoresearch Center of Ferdowsi University of Mashhad, Iran

ARTICLE INFO

Keywords:
Spin-dependent transport
Spin transfer torque
Green function's technique
Silagraphene

ABSTRACT

We theoretically investigate the spin-dependent transport and spin transfer torque (STT) in a system composed of a silagraphene nanoribbon ($SLNR$) connected to two ferromagnetic (FM) leads with arbitrary relative magnetization direction, using the tight-binding model in the nearest neighbor approximation within the framework of the Green function's technique and Landauer–Butticer formalism. We report numerical calculation results for conductance (G), magnetoresistance (MR), and spin transfer torque (STT) in the $FM/SLNR/FM$ junction for different strengths of ferromagnetic magnetization. It is found that the G and MR show oscillatory behavior around $E_F = 0$ and more interestingly, the magnitude of the MR reaches up to %100, which can be effectively used for sensitive switchings. In addition, it is demonstrated that STT versus Fermi energy shows noticeable peaks with moving away from Dirac point energy. The results show that the torques as a function of the angle between two magnetic electrodes (θ) show a sin-like behavior and the $G-\theta$ curve demonstrates approximately a $cosine$-like behavior, which is a function of M. Our results can provide valuable theoretical guidance to design future novel spintronic devices.

1. Introduction

The spin-transfer torque (STT) has gained a lot of interest due to the application the spin of electron in storage and sensor technology [1]. Theoretically, Ralph and Stiles introduced the physics of STT in magnetic devices [2] and others investigated the STT utilizing a spin diffusion model [3] and a mechanism of magnetization switching by including exchange interaction [4].

To put it simply, this phenomenon can be explained in a spin valve; spin-polarized electrons passing from the left ferromagnetic (FM) electrode (fixed layer) into another one (free layer) in which the magnetization deviates the left by an angle, may exert a torque which is called STT [5,6]. This torque can be strong enough to reverse the magnetization of the nanomagnet to switching procedure [7] or excite persistent magnetic precession [8,9] for microwave generation [10]. So STT has promising potential for direct application in the non-volatile random-access memory ($STT-RAM$), high-frequency spin torque oscillator (STO) [11–13], and designing microwave detectors [14–16].

On the other hand, the discovery and successful fabrication of graphene [17] has opened the door to investigate different two-dimensional structures especially from the carbon family [18–24]. We know silicon is one of the most famous elements that traditional electronics is based on it. Two-dimensional sheet of graphene-like silicon, namely planar silicene, has attracted intensive research interest due to its expected integration with silicon-based technology. The physical and chemical properties of silicene are studied based on theoretical and experimental works in recent years [25,26] and the first experimental evidence of epitaxial planar silicene is reported [27]. Also, the structural stability of various edge forms of silicene nanoribbons (SiNRs) has been theoretically investigated employing first-principles calculations [28].

Moreover, it is worth expecting that other two-dimensional graphene-like composites with different Si : C ratios (named siligraphene) indicate interesting properties. Compared to the pure two-dimensional graphene and silicene, silagraphenes provide more various arrangement patterns consisting of both C and Si atoms which have different electronic structures. By combining the density functional and tight-binding calculations, the formation of Dirac Cone (DC) band structures in SiC_3, Si_3C, and their analogous binary monolayers is considered [29]. X. Qin et al. demonstrated the formation of Dirac cones in two-dimensional planar SiC sheets [30]. The edge effects are taken into account by modifying the on-site energies and hopping integrals of the atoms on the two edges, as well [31]. Similar to graphene and

* Corresponding author.
E-mail address: roknabad@um.ac.ir (M.R. Roknabadi).

https://doi.org/10.1016/j.physe.2022.115413
Received 2 November 2021; Received in revised form 12 June 2022; Accepted 30 June 2022
Available online 6 July 2022

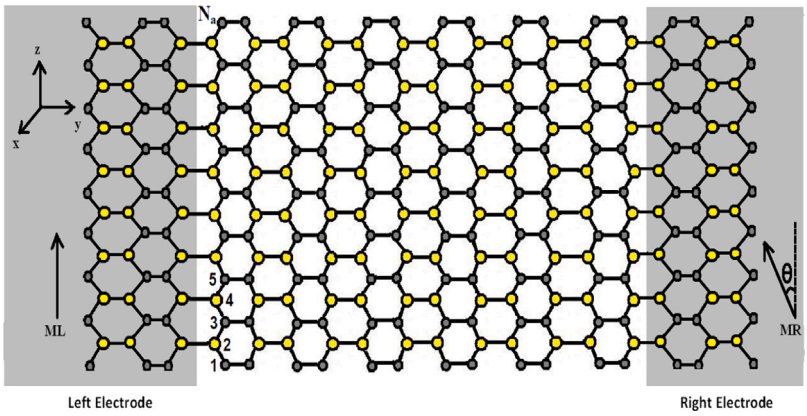

Fig. 1. Schematic view of atomic structures for SiC with right and left leads ($FM/SLNR/FM$ junction). The yellow balls represent Si and the gray balls represent C.

silicene nanoribbon, we expect the silagraphene edge configurations affect the properties of nanoribbon. For example it is shown that the silicon carbide nanoribbons with an armchair configuration exhibit three family behaviors, i.e. Na =3p, Na=3p+1, Na=3p+2 where Na is the width of the ribbon and p is a positive integer, while a silicon carbide nanoribbons with zigzag edge show half metallic behavior [32–34].

Previous works have mainly studied spin dependent transfer such as STT in two-dimensional structures like graphene [35,36] and silicene [37]. Here, we focused on SiC silagraphene which is considered in Ref. [30]. They studied different possible types of SiC silagraphene with various Si/C arrangement patterns and found that some of them have planar structures that are energetically most stable and possess Dirac cones. Our favorite structure contains C–C and Si–Si atom pairs connected by C–Si bonds that all C–C and Si–Si pairs align parallel to each other. The system has planar structure and shows Dirac cones. The thermal conductivities of the system are calculated by L. Wang and H. Sun as well [38].

With this motivation, in the present work, we focus on a system based on the SiC silagraphene nanoribbons ($FM/SLNR/FM$). We report numerical calculations using the tight-binding model in the nearest neighbor approximation within the framework of the Green function's technique and Landauer–Butticer formalism [39]. At first, conductance (G) in parallel and antiparallel configurations versus E_F is calculated and it is demonstrated that G oscillates around zero energy but does not show a symmetric behavior around the axis of $E_F = 0$. Next, we study STT versus E_F and the angle (θ) between two electrodes for different strengths of ferromagnetic magnetization. It is demonstrated that STT per unit of bias voltage (in unit of $e/4\pi$) as a function of the Fermi energy, reduces around the Dirac point energy, noticeably. Also, we see that the STT per unit of the bias voltage τ/V (in units of $e/4\pi$) versus the angle between two magnetic electrodes shows a sin-like behavior which is enhanced by increasing M.

Finally, we study G as a function of the angle (θ) between two magnetic electrodes and also around Dirac point energy to consider the system in details. We conclude that the n-type impurity is better selection to dope the system. Our results have the potential to apply to the development of the nanoelectronic field.

2. Method

The system under study consists of a silagraphene nanoribbon ($SLNR$) connected to two FM silagraphene leads (Fig. 1), where the hard wall condition is imposed on two armchair edges of the $SLNR$. We notice that the nanoribbon width (N_a) is defined as the number of dimer lines along the ribbon direction and so the system under study has $N_a = 17$. In this junction, the magnetization of the left FM lead (M_L) is assumed to be parallel to the Z-axis, while the moment of the right FM lead (M_R) deviates from the Z-direction by a relative angle θ in the XZ plane relative to M_L; that is, $\overrightarrow{M_L} = M_L(0, 0, 1)$ and $\overrightarrow{M_R} = M_R(\sin\theta, 0, \cos\theta)$.

It is worthwhile to note that the FM silagraphene leads can be realized by growing on a FM insulator or by applying an in-plane magnetic field parallel to the silagraphene layer like Ref. [37,40]. For simplicity, the influence of magnetic ordering in the leads on the central channel is neglected. Therefore the total Hamiltonian of the system is

$$H = H_c + H_{R/L} + H_{TR/TL} \tag{1}$$

where H_C describes the central $SLNR$ channel, $H_{(R/L)}$ is the Hamiltonian of the left/right FM lead and $H_{(TR/TL)}$ is the Hamiltonian for the coupling between $SLNR$ and leads. In the tight binding approximation, these partial Hamiltonians can be written as

$$H_C = \sum_{i\in C} E_C C^+{}_{i\sigma}\sigma_I C_{i\sigma} - \sum_{i,j\in C} t_C C^+{}_{i\sigma}\sigma_I C_{j\sigma} \tag{2}$$

$$H_{R/L} = \sum_{i\in R/L} E_{R/L} a^+{}_{i\sigma}\sigma_I a_{i\sigma} - \sum_{i,j\in R/L} t_{R/L} a^+{}_{i\sigma}\sigma_I a_{j\sigma} - \sum_{i\in R/L} a^+{}_{i\sigma}(\sigma.M_{R/L})a_{i\sigma} \tag{3}$$

$$H_{TR/TL} = \sum_{i\in C, j\in R/L} E_{R/L} t_{CR/CL} C^+{}_{i\sigma}\sigma_I a_{j\sigma} \tag{4}$$

where $\sigma = \uparrow (\downarrow)$ respects the spin up (down) state of electrons, $C^+{}_{i\sigma}(C_{i\sigma})$ and $a^+{}_{i\sigma}(a_{i\sigma})$ are the creation (annihilation) operators associated with the electron in the $SLNR$ region and leads, respectively. $\sigma = (\sigma_x, \sigma_y, \sigma_z)$ shows the Pauli matrices and σ_I is a 2×2 unitary matrix. E_C and $E_{(R/L)}$ are the on-site energies in the $SLNR$ channel and the left/right lead, respectively. We work in the nearest neighbor approximation and t_C is the hopping energy in the $SLNR$ channel between C–C and C–Si. $t_{(R/L)}$ and $t_{(CR/CL)}$ are the hopping energy in left/right leads and the coupling strength between the $SLNR$ channel and leads, respectively. The Fermi energy was also set to zero, i.e. $E_F = 0$.

To proceed, we apply the unitary transformation with $\hat{a}_{i\sigma} = Ra_{i\sigma}$ for all sites i in the right FM lead, where the unitary matrix R consists of the relative angle of the magnetizations θ;

$$R = \begin{pmatrix} \cos(\theta/2) & \sin(\theta/2) \\ \sin(\theta/2) & -\cos(\theta/2) \end{pmatrix} \tag{5}$$

Under this unitary transformation, the Hamiltonians H_C, H_L and H_{TL} remain unchanged, while H_R and H_{TR} become diagonal in the spin space; i.e the magnetization direction of the right FM lead is along the direction of Z-axis [37,40] as

$$H_R = \sum_{i\in R} a^+{}_{i\sigma}(E_R\sigma_I + \sigma.M'_R)a_{i\sigma} - \sum_{i,j\in R} t_R a^+{}_{i\sigma}\sigma_I a_{j\sigma} \tag{6}$$

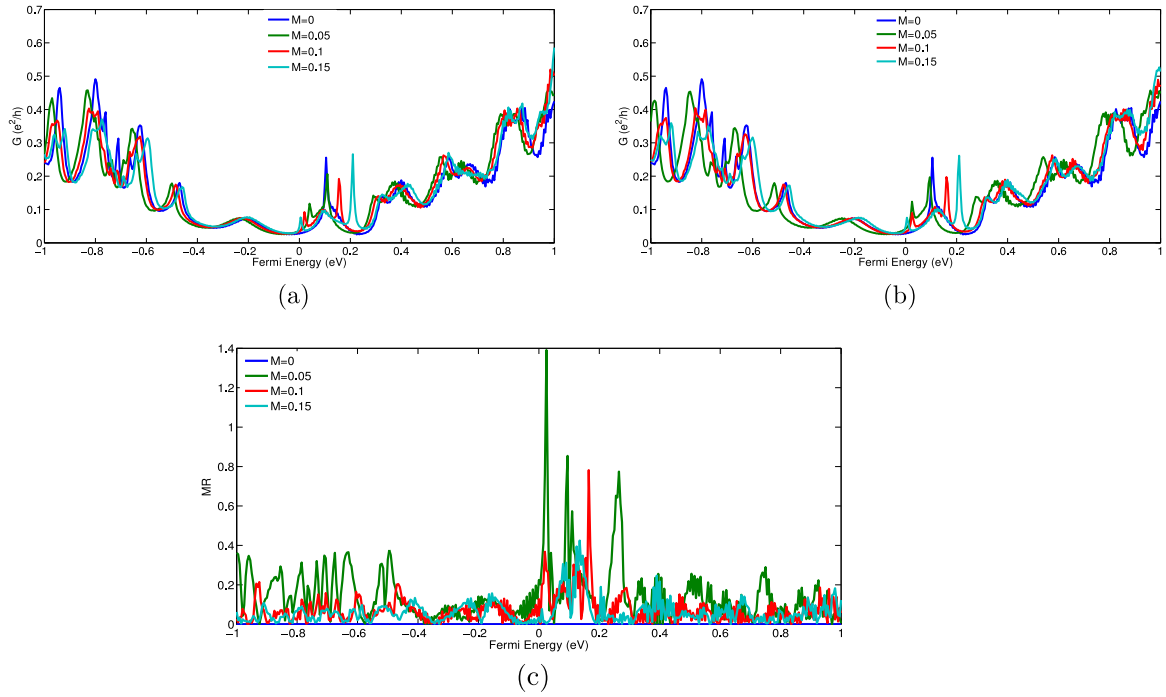

Fig. 2. Conductance, G, for (a) P ($\theta = 0$) and (b) AP ($\theta = \pi$) configurations, and (c) MR as a function of the Fermi energy (E_F) for different magnetization strengths (M).

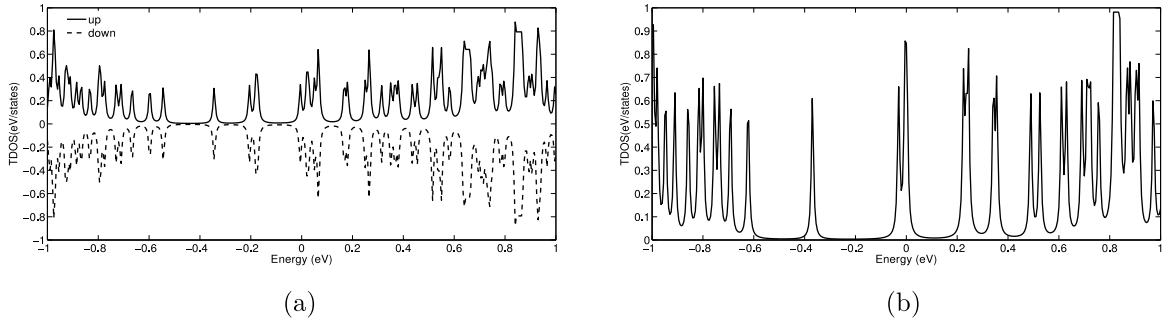

Fig. 3. The total density of states ($TDOS$) per site, for (a) central part of the system and (b) magnetic electrodes at $M = 0.1$.

$$H_{TR} = -\sum_{i\in C, j\in R} a^{+}{}_{i\sigma} R a_{j\sigma} \tag{7}$$

where $\overrightarrow{M'_R} = M_R(0, 0, 1)$. Then, the spin-dependent electronic transmission coefficient through the channel region is calculated from the Landauer–Butticer formalism:

$$T(E)_\sigma = Tr[\Gamma(E)^L_\sigma G(E)^r_\sigma \Gamma(E)^R_\sigma G(E)^a_\sigma] \tag{8}$$

where $G(E)^r_\sigma = [G(E)^r_\sigma]^+ = [EI - H_C - \Sigma^r{}_{L\sigma} - \Sigma^r{}_{R\sigma}]^{-1}$ is the retarded Green function with unit matrix I and spin index σ, where $\Sigma^r{}_{L\sigma(R\sigma)}$ is the left (right) lead retarded self-energy function in spin space [37]. Note that the effect of semi-infinite electrodes on the Hamiltonian of system is described using the self-energy terms. The self-energies are calculated iteratively [41]. $\Gamma_{(L/R)}$ is the linewidth function which can be expressed as $\Gamma_{(L/R)\sigma} = i[\Sigma^r_{(L/R)\sigma} - (\Sigma^r_{(L/R)\sigma})^+]$ [40]. Now total conductance for the junction can be obtained as $T(E) = \frac{e^2}{h}\sum_\sigma T(E)_\sigma$. Also we calculate MR by using $MR = (G_P - G_{AP})/G_P$, where $G_P(G_{AP})$ is conductance for parallel (antiparallel) spin configuration of magnetization in two electrodes. On the other hand, the STT is the time evolution rate of the total spin of the left or right FM lead which is composed of two parts; in-plane and out-of-plane STT [41]. We neglect out-of-plane coefficient which is too small in comparison with in-plane one. So the STT through the junction can be expressed as

$$\tau = \frac{1}{4\pi} Tr \int dE[G(E)^r \Gamma(E)_L G(E)^a \Gamma(E)_R] \times \times(\sigma_x \cos\theta - \sigma_z \sin\theta)[f(E)_L - f(E)_R] \tag{9}$$

where σ_x and σ_z are the Pauli matrices. Although the relationship between STT and bias Voltage (V) is nonlinear, but in very small voltage and zero Temperature, we can take a linear response for in plane STT as [37]

$$\tau/V = \frac{1}{4\pi} Tr[[G(E)^r \Gamma(E)_L G(E)^a \Gamma(E)_R] \times (\sigma_x \cos\theta - \sigma_z \sin\theta)] \tag{10}$$

To understand the behavior of the system, we make the following step-by-step analyses and hope that these achievements can be used in designing future spintronic devices.

3. Results and discussions

Following the above procedure, the results of some numerical examples of the calculated G, MR, and STT are reported in this section. In the calculations, the two ferromagnetic leads are assumed to be made of the same materials, i.e. $M_L = M_R = M$, and we assume the tunneling current flows along the y-axis. The system ($FM/SLNR/FM$ junction) is depicted in Fig. 1 symbolically.

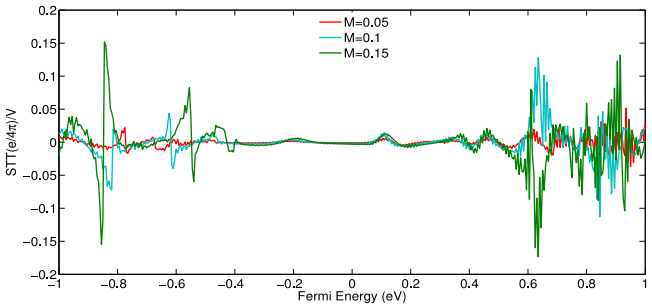

Fig. 4. The STT per unit of bias voltage V versus the Fermi energy (E_F) at $\theta = \pi/3$ for different magnetization strengths (M).

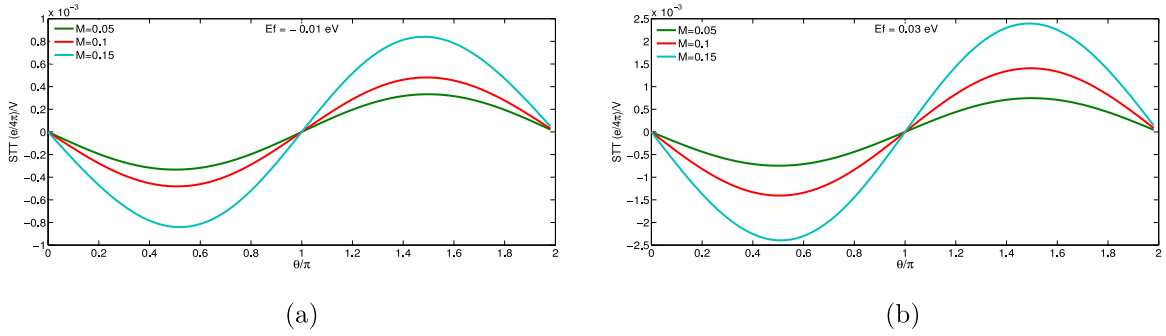

Fig. 5. The STT (in unit of $e/4\pi$) per unit of bias voltage V versus relative orientation angle θ at (a) $E_F = -0.01$ eV and (b) $E_F = 0.03$ eV for different magnetization strengths (M).

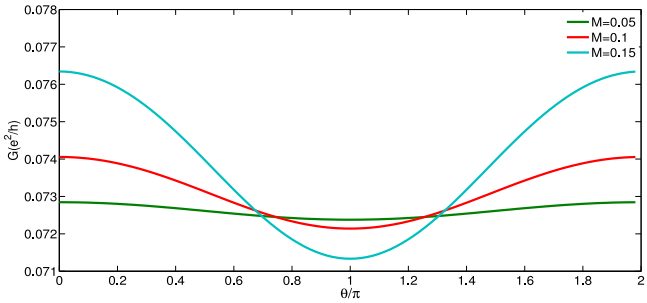

Fig. 6. The conductance G versus the relative orientation angle θ at $E_F = -0.1$ eV for different magnetization strengths (M).

In addition, the physical quantities in Hamiltonians are adapted from Ref. [30], where E_C and E_{Si} are the on-site energies of C and Si and t_C, t_{Si} and t are the hopping energies of C–C, Si–Si, and C–Si, respectively. These TB parameters are obtained fitting to reproduce the DFT band structures, $E_C = -1.164$ eV, $E_{Si} = 0.649$ eV, $t_C = 2.225$ eV, $t_{Si} = 1.241$ eV, and $t = 1.433$ eV.

In Fig. 2(a)–2(c), we present the conductance G (in units of e^2/h) in parallel configuration ($\theta = 0$) and antiparallel configuration ($\theta = \pi$), and also the magnetic resistance (MR) versus the Fermi energy E_F (in units of eV) for different magnetization strengths M (in units of eV), respectively.

Firstly, it is clearly seen that the conductance shows an oscillatory behavior with sharp peaks around zero energy which is consistent with the previous studies on graphene-based junctions [36,42]. However, in the previous works, it was shown that the G and MR curves are quite symmetric for graphene [36,42,43] and silicene [37] systems, while our results are asymmetric (Fig. 2(a), 2(b)). The origin of this different behavior can be understood according to the total density of states ($TDOS$) per site for the central region and magnetic electrodes (Fig. 3(a), 3(b)), separately. We can explicitly see that the $TDOS$ curves exhibit an asymmetric shape with sharp peaks around $E_F = 0$. So generally, one can clearly expect that the conductance follows an asymmetric and oscillatory behavior as well. Furthermore, we can observe that G is enhanced by increasing E_F due to the presence of the more and longer peaks in the $TDOS$ curves. What is more, one notices that the conductance in Fig. 2, can reach up to ~ 0.5 which is similar to the measured value for armchair-edge graphene nanoribbons between ferromagnetic leads [36], while higher G values appear at zigzag edge systems [37,42]. It seems a reasonable assumption to say that this difference originates from the role of the edge boundaries in the physical properties of the nanoribbons [44].

Next, we numerically present STT per unit of bias voltage (in unit of $e/4\pi$) as a function of the Fermi energy with different magnetization strengths at $\theta = \pi/3$. As illustrated in Fig. 4, we see an apparent visible reduction in the torque around the Dirac point energy while with moving away from $E_F = 0$, the peaks of τ/V become sharper and more noticeable. A similar result is obtained in the graphene [45] and silicene [37] systems. The torque is proportional to the polarization strength of FMs [46], and therefore we see that the peaks of τ/V become more remarkable with the increase of M.

We know that Fermi energy can be changed by doping impurity or gating the system. However, we should notice that these changes cannot be too much, because the stability of the system vanishes. So, we try to focus around $E_F = 0$. In what follows, in Fig. 5, we

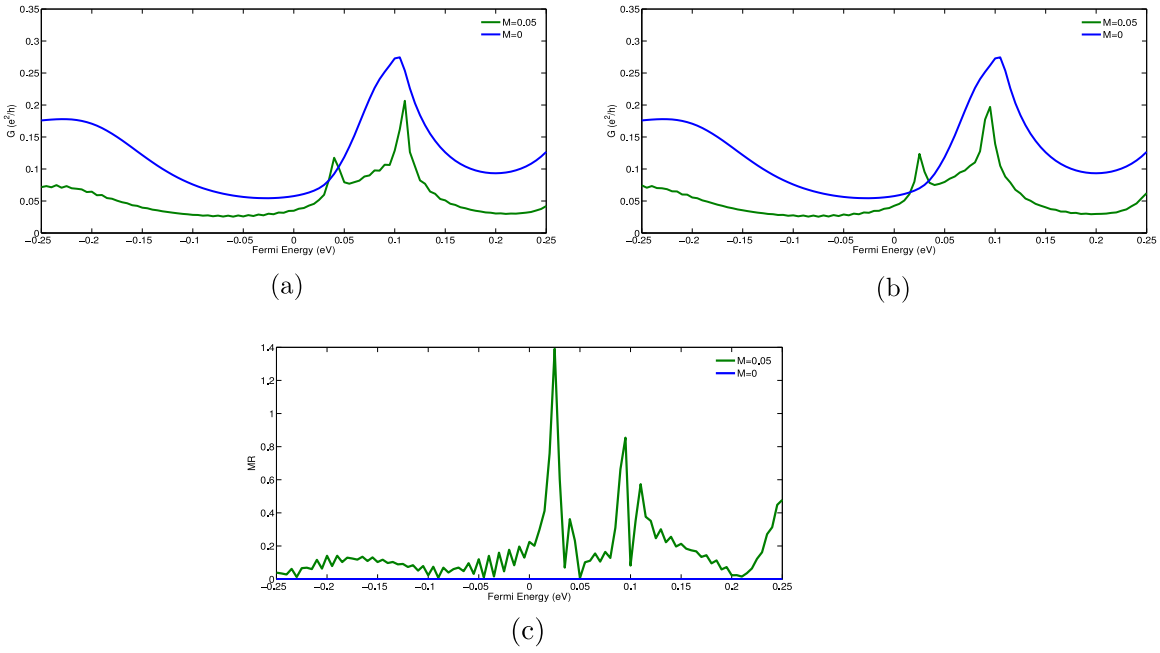

Fig. 7. Conductance, G, for (a) $P(\theta = 0)$ and (b) $AP(\theta = \pi)$ configurations, and (c) MR as a function of the Fermi energy (E_F) for $M = 0, 0.05$.

plot STT per unit of the bias voltage τ/V (in units of $e/4\pi$) versus the angle between two magnetic electrodes at $E_F = -0.01$ eV and $E_F = 0.03$ eV. As expected, it is seen that the torque shows a sin-like behavior which is similar to the previous numerical calculations for graphene [43], silicene [34], and quantum dot [47]. This is because the STT is proportional to $M_R \times (M_L \times M_R)$ which leads to generate a factor $\sin\theta$. Therefore torque vanishes for collinear alignment ($\theta = 0, \pi$) of the two FMs and definitely no longer exists with $M = 0$ (not shown here). Once again, it is clearly seen that the torque is enhanced by increasing M due to its proportionality to the polarization strength of FMs [46].

What is more, the conductance, G, is also calculated as a function of the angle θ (in units of π) for different magnetization strengths, M, where θ is the relative angle of the magnetization in the two FMs. In Fig. 6, it is demonstrated that the shape of the curves $G - \theta$ is approximately a cosin-like function regardless of the parameters M, which is similar to that of the graphene [42] and silicene [37] junctions. We notice that the range of the conductance curves enhances by increasing M, where angle θ changes from 0 to 2π. It is clear that the G is independent on θ for $M = 0$ (not shown here), as well.

Finally we go further to reach more practical results. Generally we know the change of Fermi energy is too difficult. So, it is reasonable that the calculations focus on around Fermi energy. Fig. 7 shows the conductance for parallel ($\theta = 0$) and antiparallel ($\theta = \pi$) and also MR as a function of the Fermi energy close to $E_F = 0$. Here the G and MR have been calculated just for $M = 0, 0.05$ to consider the behavior of the system in the region of Fermi energy in detail.

As expected, we can see oscillatory behavior with notable peaks for conductance in Fig. 7(a) and (b). There is one outstanding peak in nonmagnetic system ($M = 0$) which divide into two peaks with different height for M=0.05. We can explain this event by means of Zeeman term which appears in the Hamiltonian of ferromagnetic leads (Equ.3). Zeeman Effect can annihilate the degeneracy of the energy levels and split the initial peak. The effect of Zeeman term enters in the calculations by means of self-energies. Moreover by increasing M, the distance between the mentioned peaks will become more and more, because the Zeeman Effect will be more effective.

Now look at the MR curve (Fig. 7(c)). We can see some sharp peaks which are definitely located above Fermi energy and one of them is taller and has a smaller width relative to its length. Here, MR can reaches up to %100 and consequently, we can use this structure for sensitive switching.

Additionally, we should emphasize that the sharp peaks are located above $E_F = 0$ in this system. So we can conclude that the n-type impurity is more suitable for doping the system, because the n-type impurity can increase the number of electrons in the system and then the Fermi energy rise to higher magnitudes. Thus for example, we suggest that one can consider the effect of the presence of Nitrogen atoms on the transport properties of the structure under study.

4. Summery

In summary, we have theoretically investigated the conductance (G), magnetoresistance (MR) and spin transfer torque (STT) in a silagraphene-based junction ($FM/SLNR/FM$) with arbitrary relative magnetization direction. The study was performed using the Green function's technique and Landauer–Butticer formalism for different magnetization strengths (M). It is demonstrated that the conductance shows an oscillatory behavior with sharp peaks around zero energy, but the curves are antisymmetrical to the axis of $E_F = 0$ (the Dirac point), which is opposite to the previous findings for graphene and silicene systems. In order to understand the mentioned results, we present the total density of states ($TDOS$) per site for the central region and magnetic electrodes, separately. It is found that the asymmetry originates from antisymmetrical behavior of the $TDOS$ curves due to the presence of C and Si atoms in the unit cell.

In addition, we investigate STT per unit of bias voltage (in unit of $e/4\pi$) versus Fermi energy and the results show a noticeable reduction in the torque around the Dirac point energy. Furthermore, we study STT and G as a function of angle θ for different magnetization strengths M, where θ is the relative angle of the magnetization in the two FMs. Expectedly, the $STT - \theta$ curves demonstrate a sin-like behavior and the $G - \theta$ curve shows a cosin-like function regardless of the parameters M, which is similar as that for the graphene and silicene junctions. Finally, we consider G around Dirac point energy and it is demonstrated that the Zeeman Effect can split the initial peak in the presence of the magnetic leads. Our study provides a theoretical guide for designing the future nanoelectronic devices.

Declaration of competing interest

The authors declare that they have no known competing financial interests or personal relationships that could have appeared to influence the work reported in this paper.

Acknowledgments

The authors are grateful to M. Modaresi for very useful suggestions. We also thank F. Ahmadi for helpful discussions.

References

[1] H. Liu, Spin Transfer Driven Magnetization Dynamics in Spin Valves and Magnetic Tunnel Junctions (Ph.D. thesis), New York University, 2013.
[2] D.C. Ralph, M.D. Stiles, Spin transfer torques, J. Magn. Magn. Mater. 320 (2008) 1190–1216.
[3] C. Abert, et al., Field- and damping-like spin-transfer torque in magnetic multilayers, Phys. Rev. Appl. 7 (2017) 054007.
[4] S. Zhang, P.M. Levy, A. Fert, Mechanisms of spin-polarized current-driven magnetization switching, Phys. Rev. Lett. 88 (23) (2002).
[5] C. Ortiz Pauyac, Spin Torques in Systems with Spin Filtering and Spin–Orbit Interaction (Ph.D. thesis), King Abdullah University of Science and Technology, 2016.
[6] A. Brataas, A.D. Kent, H. Ohno, Current-induced torques in magnetic materials, Nature Mater. 11 (2012).
[7] S. Zhang, P.M. Levy, A. Fert, Mechanisms of spin-polarized current-driven magnetization switching, Phys. Rev. Lett. 88 (23) (2002).
[8] Y. Cui, Characterization of Magnetic Dynamics Excited by Spin Transfer Torque in a Nanomagnet (Ph.D. thesis), Cornell University, 2012.
[9] J.C. Slonczewski, Current-driven exitation of magnetic multilayers, J. Magn. Magn. Mater. 159 (1996) L1–L7.
[10] O. Boulle, et al., Shaped angular dependence of the spin-transfer torque andmicrowave generation without magnetic field, Nat. Phys. 3 (2007).
[11] I. Ying Loh, Mechanism and Assessment of Spin Transfer Torque (STT) Based Memory (Master thesis), University of Malaya, 2007.
[12] Emanuele Bosoni, Material Selection for Spin-Transfer-Torque Magnetic Random Access Memories: A High-Throughput Approach (Ph.D. thesis), Trinity College Dublin, 2020.
[13] Liliana Buda-Prejbeanu, Modelling of spintronic devices: from basic operation mechanisms toward optimization, in: Physique [physics], Communauté Université Grenoble Alpes, 2017.
[14] O.V. Prokopenko, et al., Spin-Torque Microwave Detectors: Fundamentals and Applications, MSMW'13, Kharkov, Ukraine, June 23–28, 2013.
[15] B.M. Yao, et al., Rapid microwave phase detection based on a solid state spintronic device, Appl. Phys. Lett. 104 (2014) 062408.
[16] X. Fan, et al., Magnetic tunnel junction based microwave detector, Appl. Phys. Lett. 95 (2009) 122501.
[17] D.S.L. Abergel, et al., Properties of graphene: a theoretical perspective, Adv. Phys. 59 (4) (2010) 261–482.
[18] Q. Tang, Z. Zhou, Z. Chen, Innovation and discovery of graphene-like materials via density-functional theory computations, Adv. Rev. 5 (2015).
[19] J.-C. Guo, et al., D3h X3Li3+ (X = C, Si and Ge): Superalkali cations containing three planar tetracoordinate X atoms, Computational and Theoretical Chemistry 1083 (2016) 1–6.
[20] Y. Cai, C.-P. Chuu, C.M. Wei, M.Y. Chou, Stability and electronic properties of two-dimensional silicene and germanene on graphene, Phys. Rev. B 88 (2013) 245408.
[21] L. Wu, et al., Structural and electronic properties of two-dimensional stanene and graphene heterostructure, Nanoscale Res. Lett. 11 (2016) 525.
[22] A. Acun, et al., Germanene: the germanium analogue of graphene, J. Phys.: Condens. Matter 27 (2015) 443002, (11pp).
[23] B. van den Broek, et al., Functional silicene and stanene nanoribbons compared to graphene: electronic structure and transport, 2D Materials 3 (2016) 015001.
[24] Y. Wang, Yi. Ding, Strain-induced self-doping in silicene and germanene from first-principles, Solid State Commun. 155 (2013) 6–11.
[25] J. Zhuang, et al., Honeycomb silicon: a review of silicene, Mater. Sci. http://dx.doi.org/10.1007/s11434-015-0880-2.
[26] Mubashir A. Kharadi, et al., review—silicene: from material to device applications, ECS J. Solid State Sci. Technol. 9 (2020) 115031.
[27] A.S. Dybala, et al., Planar silicene: a new silicon allotrope epitaxially grown by segregation, Adv. Funct. Mater. 1906053 (2019).
[28] S.M. Aghaei, et al., Structural stability of functionalized silicene nanoribbons with normal, reconstructed, and hybrid edges, J. Nanomater. (2016) Article ID 5959162.
[29] X. Qin, et al., Origins of Dirac cone formation in AB3 and A3B (A, B = C, Si, and Ge) binary monolayers, Sci. Rep. 7 (2017) 10546.
[30] X. Qin, et al., Origin of dirac cones in SiC silagraphene: a combined density functional and tight-binding study, J. Phys. Chem. Lett. 6 (2015) 1333–1339.
[31] K. Zhao, et al., Tight-binding model for the electronic structures of SiC and BN nanoribbons, Physica E 43 (2010) 440–445.
[32] K. Zhao, et al., Tight-binding model for the electronic structures of SiC and BN nanoribbons, Physica E 43 (2010) 440–445.
[33] L. Sun, et al., Electronic structures of SiC nanoribbons, J. Chem. Phys. 129 (2008) 174114.
[34] Y. He, et al., Adjusting the electronic properties of silicon carbide nanoribbons by introducing edge functionalization, RSC Adv. 4 (2014) 35042.
[35] B. Zhou, et al., Magnetotransport and current-induced spin transfer torque in a ferromagnetically contacted graphene, J. Phys.: Condens. Matter 22 (2010) 445302, (8pp).
[36] B. Zhou, et al., Spin-dependent transport for armchair-edge graphene nanoribbons between ferromagnetic leads, J. Phys.: Condens. Matter 23 (2011) 135304, (9pp).
[37] B. Zhou, et al., Spin-dependent transport and current-induced spin transfer torque in a disordered zigzag silicene nanoribbon, Physica B 309563 (2016).
[38] L. Wang, et al., Thermal conductivity of silicon and carbon hybrid monolayers: a molecular dynamics study, J. Mol. Model. 18 (2012) 4811–4818.
[39] S. Datta, Electronic Transport in Mesoscopic Systems, Cambridge University Press, Cambridge, England, 1995.
[40] B. Zhou, et al., Seebeck effects in a graphene nanoribbon coupled to two ferromagnetic leads, J. Appl. Phys. 115 (2014) 114305.
[41] M. Modarresi, et al., Transport properties of an armchair boron-nitride nanoribbon embedded between two graphene electrodes, Physica E 43 (2011) 1751–1754.
[42] Jiang chai Chen, et al., Electronic transport through a graphene-based ferromagnetic/normal/ferromagnetic junction, J. Phys.: Condens. Matter 22 (2010) 035301, (8pp).
[43] B. Zhou, et al., Magnetotransport and current-induced spin transfer torque in a ferromagnetically contacted graphene, J. Phys.: Condens. Matter 22 (2010) 445302, (8pp).
[44] Electronic states of graphene nanoribbons and analytical solutions, katsunori wakabayashi, ken-ichi sasaki, takeshi nakanishi and toshiaki enoki, Sci. Technol. Adv. Mater. 11 (2010) 054504, (18pp).
[45] Kai-He Ding, et al., Spin-dependent transport and current-induced spin transfer torque in a strained graphene spin valve, Phys. Rev. B 89 (2014) 195443.
[46] J.C. Slonczewski, Current-driven excitation of magnetic multilayers, J. Magn. Magn. Mater. 159 (1996).
[47] L. Qin, Y. Guo, Current and spin torque in a ferromagnet-quantum dot-ferromagnet tunneling system: quantum rate equations, Eur. Phys. J. B 63 (2008) 211–218.